Bidirectional surface photovoltage on a topological insulator

T. Yoshikawa,[1] K. Sumida,[1] Y. Ishida,[2,*] J. Chen,[1] M. Nurmamat,[1] K. Akiba,[2] A. Miyake,[2] M. Tokunaga,[2] K. A. Kokh,[3,4,5] O. E. Tereshchenko,[4,5,6] S. Shin,[2] and A. Kimura[1,†]

[1]*Graduate School of Science, Hiroshima University, 1-3-1 Kagamiyama, Higashi-Hiroshima, Hiroshima 739-8526, Japan*

[2]*ISSP, University of Tokyo, 5-1-5 Kashiwa-no-ha, Kashiwa, Chiba 277-8581, Japan*

[3]*Sobolev Institute of Geology and Mineralogy, Siberian Branch, Russian Academy of Sciences, 3, Koptyug avenue, 630090 Novosibirsk, Russia*

[4]*Novosibirsk State University, ulica Pirogova 2, 630090 Novosibirsk, Russia*

[5]*Saint Petersburg State University, 1, Ulyanovskaya strasse, Saint Petersburg 198504, Russia*

[6]*IRzhanov Institute of Semiconductor Physics, Siberian Branch, Russian Academy of Sciences, 13, Lavrentiev avenue, 630090 Novosibirsk, Russia*

(Received 27 January 2017; revised manuscript received 7 April 2017; published 31 October 2019)

Controlled extraction of spin-polarized currents from the surface of topological insulators (TIs) would be an important step to use TIs as spin-electronic device materials. One way is to utilize the surface photovoltage (SPV) effect, by which the surface current may flow upon irradiation of light. To date, unipolar SPV has been observed on TIs, while the realization of ambipolar SPV is crucial for taking control over the direction of the flow. By using time-resolved photoemission, we demonstrate the ambipolar SPV realized on the TI Bi_2Te_3. The topological surface states showed downward and upward photovoltaic shifts for the *n*- and *p*-type samples, respectively. We also discerned the photogenerated carriers accumulated in the surface states for >4 μs. We provide the keys besides the in-gap Fermi level to engineer the SPV on TIs.

DOI: 10.1103/PhysRevB.100.165311

I. INTRODUCTION

Topological insulators (TIs) possess spin-polarized metallic states on the surface as a result of the nontrivial topology of the bulk band structure [1]. The surface of TIs is thus considered as a promising platform for spin-electronic functions. Generating spin-polarized surface currents out of the spin-polarized metallic states would be a milestone function, and optical means provides several pathways to this end. One way is to utilize the photogalvanic effect, by which the currents may be generated by illuminating circularly polarized light [2,3], and the mechanism behind is under scrutiny [3–5]. An acceleration of topological surface electrons has been demonstrated with sub-cycle THz light wave, which could be utilized to generate spin polarized current [6]. Another way is to utilize the surface photovoltage (SPV) effect, as proposed recently [7,8]. The idea is to shine light in the surface band bending region developed on the edge of so-called bulk-insulating TIs; see Fig. 1. Similar to the generation of photovoltage in solar-cell batteries, voltaic change can be induced on the illuminated area of surface through the SPV effect. Because the surface is intrinsically metallic, surface current will either flow out of or into the illuminated area from the dark surroundings depending on the polarity of the SPV, and because the surface states are spin polarized, the photogated surface current will also be spin polarized.

For the SPV to emerge on TI surface, the locus of Fermi level (E_F) has to be in the bulk energy gap. Then, the surface band bending can be developed on the interface of metallic surface and semiconducting bulk. To date, SPVs as large as 0.1 eV have been observed on a bulk-insulating TI Bi_2Te_2Se [8,9]. Enhancement of SPV was also demonstrated via optical aging due to a progressed subsurface band bending [10]. For practical application, realization of a bidirectional SPV is crucial for taking full control of the surface current by light. However, the substantial subsurface band bending caused through the impurity band that pins E_F as well as the temperature-dependent carrier type that causes an unstable SPV have certainly prevented Bi_2Te_2Se from an ideal ambipolar control of SPV [9].

Bi_2Te_3 is an exemplary TI [11,12], and is also well known as a thermoelectric material [13] and a stable carrier type in a wide temperature range is confirmed (see the Supplemental Material) [14]. We show that the ambipolar SPV can be realized in the carrier-type-controlled Bi_2Te_3 [15,16]. By using time- and angle-resolved photoemission spectroscopy (TARPES) implemented by the pump-probe method, we observe downward and upward photovoltaic shifts on the *n*- and *p*-type sample surfaces, respectively, and the amount of the shift is controlled by the pump power. We also observe polarity-dependent changes in the filling of the topological surface states for >4 μs. The results can be nicely explained by the Schottky barrier junction model. We provide keys for TIs to meet the semiconductor-junction functions, and show a way [17] to manipulate the light-induced current on TIs.

*ishiday@issp.u-tokyo.ac.jp
†akiok@hiroshima-u.ac.jp

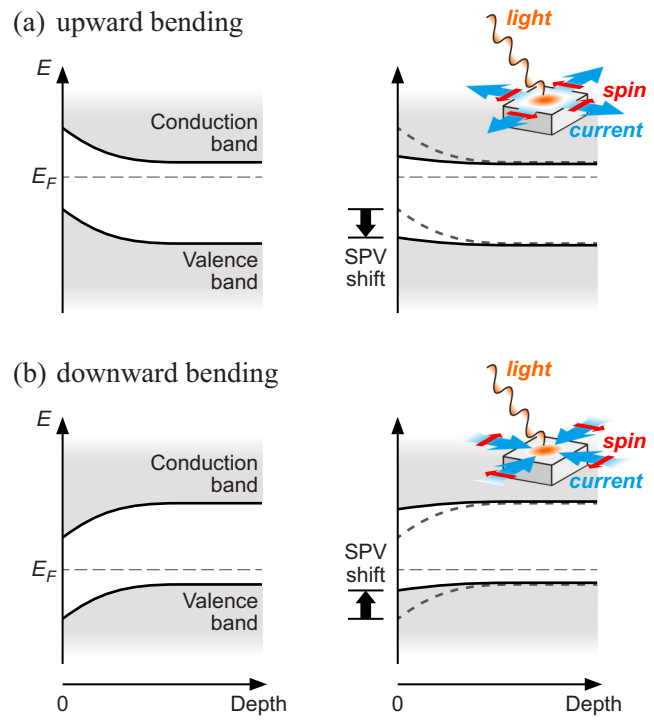

FIG. 1. The surface photovoltage effect on TIs. Conduction and valence bands bend upwards (a) and downwards (b) depending on the locus of E_F in the band gap, as shown in the left panels. When illuminated, the bending relaxes and photovoltage is generated on surface (right panels). Upper right schematics in the right panels show the flow of spin-polarized current on metallic surface of TIs out of (a) and into (b) the illuminated area.

II. EXPERIMENT

The Bi_2Te_3 samples were fabricated by using the modified Bridgman method [15,16]. By slowly cooling the slightly Te-rich melt, a gradation in the carrier concentration was formed along the crystal growth, and the resultant ingot was a natural *p*-*n* junction [15,16]. The *p*- and *n*-type samples where cut out from the ingot, and had the atomic ratios of Bi : Te = 2.04 : 2.96 and 2.01 : 2.99, respectively, which were determined through electron probe microanalysis. The *n*-type (*p*-type) sample had the carrier concentration of $\sim 1.6 \times 10^{18}$ ($\sim 9.5 \times 10^{18}$) cm^{-3} and the mobility of $\sim 5.0 \times 10^4$ ($\sim 5.2 \times 10^3$) $cm^2/V\,s$ at 10 K [14].

TARPES measurements were carried out by using a hemispherical analyzer and a Ti:sapphire laser system that delivered linearly polarized 1.5-eV pump and 5.9-eV probe pulses at the repetition rate of 250 kHz [18]. The reference of the Fermi energy E_F and the energy resolution of $\sim$15 meV were determined by recording the Fermi cutoff of gold in electrical contact to the sample and the analyzer. We reduced the probe power to <1 μW in order to minimize the space-charge broadening of the spectrum. Under the reduced power, the Fermi cutoff of the spectrum of the sample occurred at the referenced E_F within 5 meV, which indicates that both the probe-induced photovoltaic effect [19,20] and charging effect were negligibly small [14]. The origin of the pump-probe delay and the time resolution of 300 fs were determined from the TARPES signal of graphite attached next to the sample. The spot diameters of the *s*-polarized pump and *p*-polarized probe beams at the sample were 280 and 85 μm, respectively. Measurements were carried out at pressures $<5 \times 10^{-11}$ Torr and temperatures $\sim$10 K. We did not discern any aging effects during the measurements over $\sim$12 h after cleavage. The effect is known to be pronounced when the sample is rich in defects, appears as an hour-long shift of the surface bands after cleavage, and continues until the modification is completed in the subsurface region [9,10,21–23]. The absence thus indicates that the number of defects was relatively small, and the balance in the subsurface region was immediately achieved upon the cleavage.

TARPES has become a powerful tool to investigate the nonequilibrated states of matter from the electronic structure point of view. Being a surface sensitive method, TARPES has also opened pathways to explore the light-induced phenomena occurring on the edge of matter, and thus on surface of TIs [24–26]. In TARPES, a femtosecond pump pulse hits the sample and initiates dynamics; subsequently at a delay time t, a femtosecond probe pulse generates photoelectrons, whose energy-and-momentum distribution carries information of the electronic structures of the nonequilibrated state. Because the pump-and-probe event occurs repetitively, in the present case at 250 kHz (interval time of 4 μs), the method can also be used to investigate the periodic steady states, which is realized when the duration of the effect by the pump lasts more than the interval time. Since the typical duration of the photovoltage exceeds μs [27], SPVs on TIs realized in the periodic steady state can be detected by TARPES [7,8].

III. RESULT AND DISCUSSION

We first show the results for the *n*-type Bi_2Te_3 sample. Figure 2(a) displays the energy-and-momentum distribution image of the photoelectron intensity recorded without irradiating the pump pulses. Two branches of the topological surface bands are observed to cross E_F along $\bar{\Gamma}$-$\bar{M}$ at the momentum $k_F^n = 0.090$ Å^{-1} with the velocity $v_F^n = 2.7$ eV Å. The crossing point of the two branches, or the Dirac point, is located at $E_D^n = -175$ meV. The overall band structures and their visibility with the 5.9-eV probe are consistent with the literature [11,14,28]. No other bands are observed to cross E_F.

By turning on the pump, the sample is repetitively hit by the 170-fs pulses, and is driven into the periodic steady state. Figures 2(b) and 2(c) are the distribution images recorded when the sample was irradiated with the pump power $P =$ 20 mW (fluence corresponding to ~ 0.128 mJ/cm^2): The latter was recorded just after the arrival of the pump pulse ($t =$ 1.33 ps); the former was recorded at $t = -1.33$ ps, which is equivalent to recording the image at 4 μs after the arrival of the preceding pump pulse. At $t = 1.33$ ps, the bands extend into the unoccupied side, which indicates that the electrons are redistributed across E_F after the impact by the pump. Such redistributions in picoseconds are commonly observed in the TARPES studies of TIs [24–26,29,30].

The main focus in the present study is the downward shift of the spectral features in energy compared to the case without pump. For example, the features around the Dirac point is shifted for $\Delta_n = -31$ meV in both images of Figs. 2(b) and 2(c). In the image Fig. 2(b) recorded at $t \sim 4$ μs, when

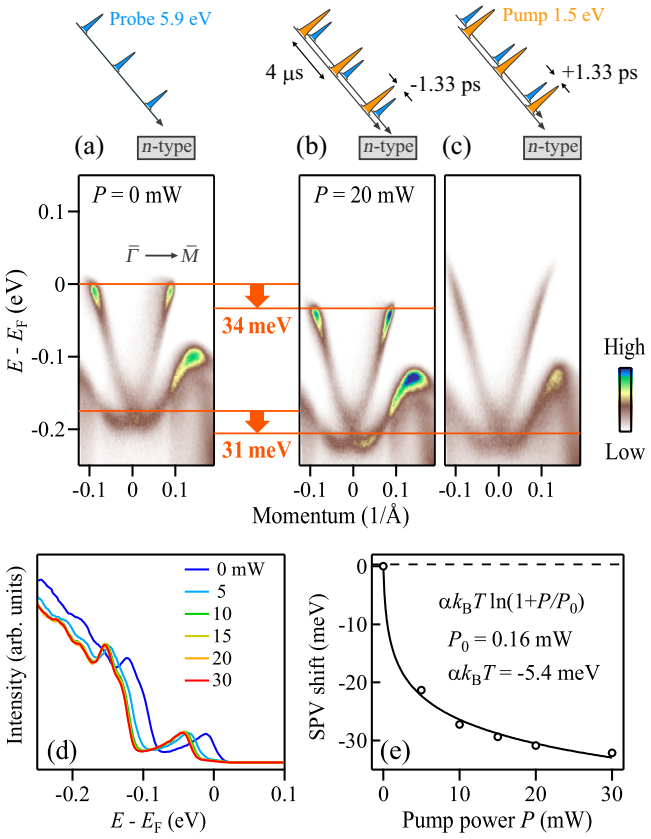

FIG. 2. Surface photovoltaic effect on n-type Bi_2Te_3. TARPES images recorded without pump (a), and with pump at $t = -1.33$ ps $\equiv \sim 4$ μs (b) and at $t = 1.33$ ps (c). Pump-probe configurations are also illustrated. (d) Momentum-integrated spectra recorded at various pump powers. (e) Shift of the Dirac point as a function of the pump power.

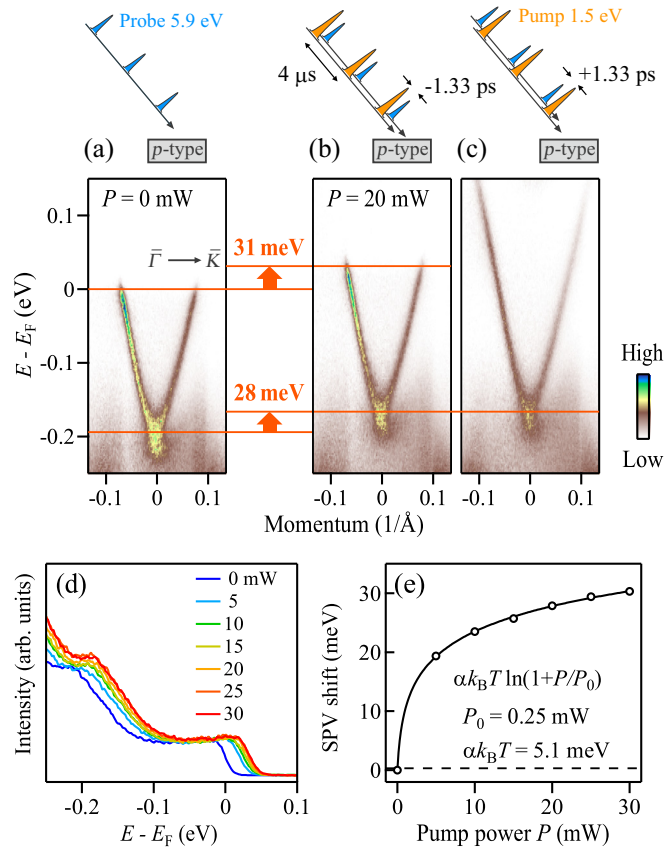

FIG. 3. Surface photovoltaic effect on p-type Bi_2Te_3. TARPES images recorded without pump (a), and with pump at $t = -1.33$ ps $\equiv \sim 4$ μs (b) and at $t = 1.33$ ps (c). Pump-probe configurations are also illustrated. (d) Momentum-integrated spectra recorded at various pump powers. (e) Shift of the Dirac point as a function of the pump power.

the electronic excitations across E_F are mostly settled, the Fermi cutoff is shifted for -34 meV. The downward shift is attributed to the emergence of SPV on the n-type Bi_2Te_3 irradiated by the pump. The difference in the downward shifts at the Fermi cutoff and at the Dirac point is attributed to the pump-induced filling of the holes in the surface states, as we discuss later. The observations herein differ from the effect reported in [29] which did not accompany the SPV shift and that did not persist for >4 μs.

Figure 2(d) shows the momentum-integrated spectra recorded at various P's. The spectral shift becomes larger at higher P's. Plotted in Fig. 2(e) is the shift of the Dirac point as a function of P. With increasing P, the shift shows the tendency of saturation, or a logarithmic increase, which we analyze later.

Next, we show the results for the p-type sample. The conical dispersion of the topological surface states are observed in the image recorded without pump [Fig. 3(a)]: The surface bands cross E_F at $k_F^p = 0.072$ Å^{-1} along $\bar{\Gamma}$-$\bar{K}$ with the velocity $v_F^p = 2.9$ eV Å, and the Dirac point occurs at $E_D^p = -194$ meV. While the structure and visibility of the bands are similar to the previous reports [11,14,28], the order $E_D^p < E_D^n$ appears opposite from what is expected from the carrier type and band alignment of the bulk. This is caused by two effects. The first is the effect due to the extended surface band bending that penetrates into the semiconducting bulk (Fig. 1). E_D^p and E_D^n could come closer or be reversed. The second is the effect that can occur through the modifications in the subsurface region that leads to quantized states [31]. These edge effects can shift E_D^p and E_D^n from the expectation. However, the subsurface band bending should play only a minor role in our samples because no quantized state appears in both n- and p-type samples due to a small number of defects by the modified Bridgman method [15,16].

When the p-type sample is pumped at $P = 20$ mW, we observe that the images [Figs. 3(b) and 3(c)] are shifted upwards in energy compared to the image recorded without pump [Fig. 3(a)]. The direction of the shift is opposite to the case for the n-type sample. The values of the shift are 28 ($\equiv \Delta_p$) and 31 meV, respectively, at the Dirac point and at the Fermi cutoff of the surface states. The momentum-integrated spectra recorded at various P's and the Dirac-point shift as a function of P are displayed in Figs. 3(d) and 3(e), respectively. The amount of the shift as well as the tendency of the saturation with increasing P is similar to the case observed on the n-type sample, but the distinction is in the direction of the shift.

We apply the Schottky barrier junction model [27,32] to explain the pump-power dependency of the shift. The model accounts for a metal-semiconductor interface, on which a band bending is formed on the semiconductor side. The photovoltage that emerges due to the relaxation of the band bending can be described as $\alpha k_B T \ln(1 + P/P_0)$ [32]. Here, α is the ideality factor, k_B is the Boltzmann constant, T ranges from 10 to 40 K concerning the heating effect (see later), and P_0 is a constant.

The theoretical curves can nicely trace the pump-induced shifts for the n- and p-type samples; see Figs. 2(e) and 3(e), in which the curves with $\alpha k_B T = -5.4$ and 5.1 meV are overlaid, respectively. The overall agreement indicates that the observed shift can be explained by the Schottky model. The sign of α indicates that an upward and downward surface band bendings were formed on the edge of the n- and p-type samples, respectively, which is consistent with the natural expectation (Fig. 1). The absolute values of α ranges from 1.5 to 6.3 concerning the laser-induced heating effect for both n- and p-type samples: α exceeding the ideal value 1 can occur in metal-semiconductor Schottky junctions at low temperatures; see [33] and references therein.

Finally, we show that the difference in the pump-induced shift of the Dirac point and the Fermi cutoff can also be explicated by the Schottky junction model. The shift of the Dirac point Δ_i ($i = n$ or p) is a measure of the light-induced relaxation of the surface band bending. In addition to the relaxation, a change in the surface state filling can occur, because the holes (electrons) that are photogenerated in the band bending region diffuse towards the edge for the n-type (p-type) sample and accumulate on surface, as shown in Fig. 4(a) [Fig. 4(b)]. The additional shift of $\delta_n = -3$ meV ($\delta_p = 3$ meV) of the Fermi cutoff to the shift at the Dirac point for the n-type (p-type) sample can thus be attributed to the accumulated holes (electrons) that are maintained for >4 μs.

The width of the surface band bending region L_i can be estimated by observing that the charge separated by the distance L_i produces the voltage $V_i = -\Delta_i/e$ (e is the unit charge). That is, $Q_i/\varepsilon = V_i/L_i$ can hold, where Q_i is the induced surface charge density and ε is the dielectric constant. Our estimation of L_i falls around $\sim$400 nm for both n- and p-type samples, in which ε at 15 K is set to 290 times the value for vacuum [34] and Q_i is derived from the increase in the Fermi-surface area $s_i = 2\pi k_F^i \delta_i / v_F^i = -Q^i/e/(2\pi)^2$ (we assumed that the Fermi surface is circular, which holds nicely in the bulk-insulating regime [11]).

Before closing, we discard the pump-induced thermoelectric effect as the possible origin of the observed shift. Pump irradiation may heat up the illuminated area on the sample. Then, the thermopower can develop between the hot spot and the cold surroundings. The pump-induced heating was at most $\Delta T = 30$ K at $P = 30$ mW, as estimated from the broadening of the Fermi cutoff observed in the image recorded at $t = 4$ μs. Because the typical value of the Seebeck coefficient is $|S| \sim 20$ μV/K at 20 K for the samples studied herein [35], the pump-induced heating can generate the thermoelectric voltage of $|S|\Delta T \sim 0.5$ mV at most. Therefore, the pump-induced shift as large as 30 meV cannot be explained by the thermoelectric effect alone, and reinforces our point of view that the shift is due to the SPV effect.

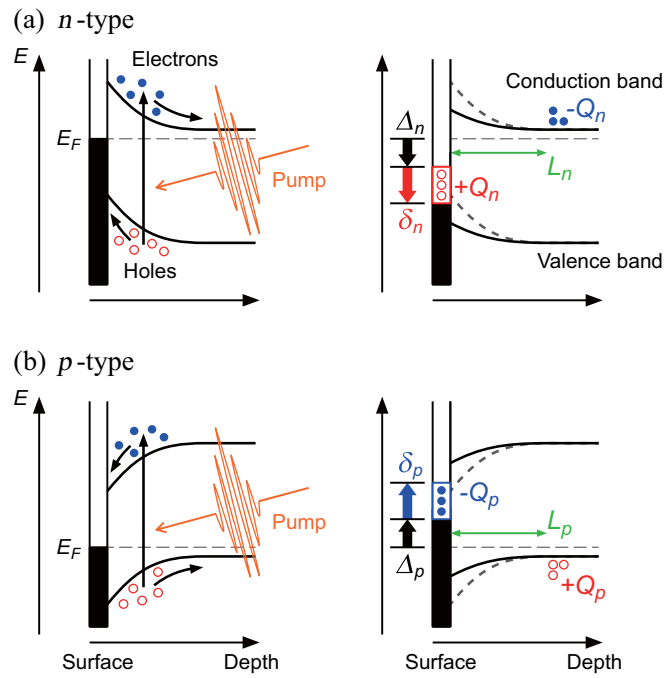

FIG. 4. Schematics of SPV and light-induced fillings in the Schottky barrier model for n- (a) and p-type (b) TIs. Left panels show the photogeneration of the carriers in the band bending region. Right panels show the photogenerated carriers separated across the band bending region.

Having demonstrated the ambipolar SPV, we became aware of another key, besides the locus of the E_F in the band gap, when taking control of the polarity: Departure becomes necessary from TIs, such as the family of Bi_2Te_2Se [36–38], whose bulk insulation is achieved through the formation of an impurity band (IB). The low-mobility IB pins E_F within the bulk band gap and works nicely for the purpose to achieve a surface-dominated transport. However, for engineering the SPV, the IB becomes an obstacle in twofold. (1) There is little controllability of the locus of the IB in the gap, and the direction of the band bending cannot be changed easily. (2) If the band pinning is too strong, surface band bendings cannot develop fully. In fact, a negligibly small SPV was experienced [39] in the TARPES study of $Bi_{1.5}Sb_{0.5}Te_{1.7}Se_{1.3}$ [37] even though it had higher resistivity to Bi_2Te_2Se [36,38] that showed the SPV shift of $\sim$0.1 eV [8]. Thus, the degree of bulk insulation alone is not a sufficient measure: TIs showing ambipolar transport provide the platform where full exploitations can be made of the semiconductor junction functions such as the SPV effect. Note that ambipolar transport was also achieved in Bi_2Se_3 recently [40]; spin polarization of the light-induced surface current may be detected by an electronic device introduced recently [17,41].

IV. CONCLUSION

In conclusion, a bidirectional photovoltaic shift has been demonstrated on the n- and p-type Bi_2Te_3 sample surface, where the amount of the shift is well controlled by the power of pump. We also observed polarity-dependent changes in the filling of the topological surface states that last for >4 μs.

The results can be nicely explained by the Schottky barrier junction model. The key is the locus of E_F in the band gap, for TIs to meet the semiconductor-junction functions. Our findings open a way to manipulate the light-induced spin polarized current on TIs.

ACKNOWLEDGMENTS

The experiments were performed at ISSP, University of Tokyo. This work was partly supported by the Bilateral Collaboration Program between RFBR (Russia) and JSPS (Japan) and also by KAKENHI Grants No. 26247064, No. 26800165, No. 17H06138, No. 18H01148, No. 18H03683, and No. 19H00651. This study was also supported by the Saint Petersburg State University (Grant No. 15.61.202.2015) and the Russian Science Foundation (Project No. 17-12-01047) in part of the single-crystal growth and structural characterization. K.A.K. was financially supported by RFBR (Grant No. 18-29-12094) and state assignment contract of IGM SB RAS. T.Y. and K.S. were financially supported by the Grant-in-Aid for JSPS Fellows No. 18J22309 and No. 19J00858, respectively.

[1] M. Z. Hasan and C. L. Kane, Rev. Mod. Phys. **82**, 3045 (2010).
[2] J. W. McIver, D. Hsieh, H. Steinberg, P. Jarillo-Herrero, and N. Gedik, Nat. Nanotechnol. **7**, 96 (2012).
[3] C. Kastl, C. Karnetzky, H. Karl, and A. W. Holleitner, Nat. Commun. **6**, 6617 (2015).
[4] L. Braun, G. Mussler, A. Hruban, M. Konczykowski, T. Schumann, M. Wolf, M. Münzenberg, L. Perfetti, and T. Kampfrath, Nat. Commun. **7**, 13259 (2016).
[5] C.-K. Chan, N. H. Lindner, G. Refael, and P. A. Lee, Phys. Rev. B **95**, 041104(R) (2017).
[6] J. Reimann, S. Schlauderer, C. P. Schmid, F. Langer, S. Baierl, K. A. Kokh, O. E. Tereshchenko, A. Kimura, C. Lange, J. Güdde, U. Höfer, and R. Huber, Nature (London) **562**, 396 (2018).
[7] Y. Ishida, T. Otsu, T. Shimada, M. Okawa, Y. Kobayashi, F. Iga, T. Takabatake, and S. Shin, Sci. Rep. **5**, 8160 (2015).
[8] M. Neupane, S.-Y. Xu, Y. Ishida, S. Jia, B. M. Fregoso, C. Liu, I. Belopolski, G. Bian, N. Alidoust, T. Durakiewicz, V. Galitski, S. Shin, R. J. Cava, and M. Z. Hasan, Phys. Rev. Lett. **115**, 116801 (2015).
[9] E. Papalazarou, L. Khalil, M. Caputo, L. Perfetti, N. Nilforoushan, H. Deng, Z. Chen, S. Zhao, A. Taleb-Ibrahimi, M. Konczykowski, A. Hruban, A. Wołoś, A. Materna, L. Krusin-Elbaum, and M. Marsi, Phys. Rev. Mater. **2**, 104202 (2018).
[10] T. Yoshikawa, Y. Ishida, K. Sumida, J. Chen, K. A. Kokh, O. E. Tereshchenko, S. Shin, and A. Kimura, Appl. Phys. Lett. **112**, 192104 (2018).
[11] Y. L. Chen, J. G. Analytis, J.-H. Chu, Z. K. Liu, S.-K. Mo, X. L. Qi, H. J. Zhang, D. H. Lu, X. Dai, Z. Fang, S. C. Zhang, I. R. Fisher, Z. Hussain, and Z.-X. Shen, Science **325**, 178 (2009).
[12] D. X. Qu, Y. S. Hor, J. Xiong, R. J. Cava, and N. P. Ong, Science **329**, 821 (2010).
[13] H. J. Goldsmid, Proc. Phys. Soc. **71**, 633 (1958).
[14] See Supplemental Material at http://link.aps.org/supplemental/10.1103/PhysRevB.100.165311 for transport measurements, energy calibration, negligibility of the probe induced effects and unoccupied band structures.
[15] K. A. Kokh, S. V. Makarenko, V. A. Golyashov, O. A. Shegaid, and O. E. Tereshchenko, CrystEngComm **16**, 581 (2014).
[16] T. Bathon, S. Achilli, P. Sessi, V. A. Golyashov, K. A. Kokh, O. E. Tereshchenko, and M. Bode, Adv. Mater. **28**, 2183 (2016).
[17] K. Kondou, R. Yoshimi, A. Tsukazaki, Y. Fukuma, J. Matsuno, K. S. Takahashi, M. Kawasaki, Y. Tokura, and Y. Otani, Nat. Phys. **12**, 1027 (2016).
[18] Y. Ishida, T. Togashi, K. Yamamoto, M. Tanaka, T. Kiss, T. Otsu, Y. Kobayashi, and S. Shin, Rev. Sci. Instrum. **85**, 123904 (2014).
[19] J. E. Demuth, W. J. Thompson, N. J. DiNardo, and R. Imbihl, Phys. Rev. Lett. **56**, 1408 (1986).
[20] M. Alonso, R. Cimino, and K. Horn, Phys. Rev. Lett. **64**, 1947 (1990).
[21] H.-J. Noh, H. Koh, S.-J. Oh, J.-H. Park, H.-D. Kim, J. D. Rameau, T. Valla, T. E. Kidd, P. D. Johnson, Y. Hu, and Q. Li, Europhys. Lett. **81**, 57006 (2008).
[22] D. Hsieh, Y. Xia, D. Qian, L. Wray, J. H. Dil, F. Meier, J. Osterwalder, L. Patthey, J. G. Checkelsky, N. P. Ong, A. V. Fedorov, H. Lin, A. Bansil, D. Grauer, Y. S. Hor, R. J. Cava, and M. Z. Hasan, Nature (London) **460**, 1101 (2009).
[23] S. V. Eremeev, M. G. Vergniory, T. V. Menshchikova, A. A. Shaposhnikov, and E. V. Chulkov, New J. Phys. **14**, 113030 (2012).
[24] J. A. Sobota, S. Yang, J. G. Analytis, Y. L. Chen, I. R. Fisher, P. S. Kirchmann, and Z.-X. Shen, Phys. Rev. Lett. **108**, 117403 (2012).
[25] Y. H. Wang, D. Hsieh, E. J. Sie, H. Steinberg, D. R. Gardner, Y. S. Lee, P. Jarillo-Herrero, and N. Gedik, Phys. Rev. Lett. **109**, 127401 (2012).
[26] A. Crepaldi, B. Ressel, F. Cilento, M. Zacchigna, C. Grazioli, H. Berger, P. Bugnon, K. Kern, M. Grioni, and F. Parmigiani, Phys. Rev. B **86**, 205133 (2012).
[27] L. Kronik and Y. Shapira, Surf. Sci. Rep. **37**, 1 (1999).
[28] M. Ärrälä, H. Hafiz, D. Mou, Y. Wu, R. Jiang, T. Riedemann, T. A. Lograsso, B. Barbiellini, A. Kaminski, A. Bansil, and M. Lindroos, Phys. Rev. B **94**, 155144 (2016).
[29] M. Hajlaoui, E. Papalazarou, J. Mauchain, L. Perfetti, A. Taleb-Ibrahimi, F. Navarin, M. Monteverde, P. Auban-Senzier, C. R. Pasquier, N. Moisan, D. Boschetto, M. Neupane, M. Z. Hasan, T. Durakiewicz, Z. Jiang, Y. Xu, I. Miotkowski, Y. P. Chen, S. Jia, H. W. Ji *et al.*, Nat. Commun. **5**, 3003 (2014).
[30] S. Zhu, Y. Ishida, K. Kuroda, K. Sumida, M. Ye, J. Wang, H. Pan, M. Taniguchi, S. Qiao, S. Shin, and A. Kimura, Sci. Rep. **5**, 13213 (2015).
[31] P. D. C. King, R. C. Hatch, M. Bianchi, R. Ovsyannikov, C. Lupulescu, G. Landolt, B. Slomski, J. H. Dil, D. Guan, J. L. Mi, E. D. L. Rienks, J. Fink, A. Lindblad, S. Svensson, S. Bao, G. Balakrishnan, B. B. Iversen, J. Osterwalder, W. Eberhardt, F. Baumberger, and P. Hofmann, Phys. Rev. Lett. **107**, 096802 (2011).

[32] D. Bröcker, T. Gießel, and W. Widdra, Chem. Phys. **299**, 247 (2004).
[33] D. Korucu, H. Efeoglu, A. Turut, and S. Altindal, Mater. Sci. Semicond. Proc. **15**, 480 (2012).
[34] W. Richter and C. R. Becker, Phys. Status Solidi B **84**, 619 (1977).
[35] P. A. Walker, Proc. Phys. Soc. **76**, 113 (1960).
[36] Z. Ren, A. A. Taskin, S. Sasaki, K. Segawa, and Y. Ando, Phys. Rev. B **82**, 241306(R) (2010).
[37] Z. Ren, A. A. Taskin, S. Sasaki, K. Segawa, and Y. Ando, Phys. Rev. B **84**, 165311 (2011).
[38] S. K. Kushwaha, Q. D. Gibson, J. Xiong, I. Pletikosic, A. P. Weber, A. V. Fedorov, N. P. Ong, T. Valla, and R. J. Cava, J. Appl. Phys. **115**, 143708 (2014).
[39] S. Kim, S. Yoshizawa, Y. Ishida, K. Eto, K. Segawa, Y. Ando, S. Shin, and F. Komori, Phys. Rev. Lett. **112**, 136802 (2014).
[40] P. Syers and J. Paglione, Phys. Rev. B **95**, 045123 (2017).
[41] C. H. Li, O. M. J. van 't Erve, J. T. Robinson, Y. Liu, L. Li, and B. T. Jonker, Nat. Nanotechnol. **9**, 218 (2014).